# AKHMEDIEV BREATHERS AS ULTRA-WIDEBAND PULSES

**B. Varlot,[1] Y. Chembo,[2] and C. Finot[1]**
[1] Laboratoire Interdisciplinaire CARNOT de Bourgogne, UMR 6303 CNRS-Université de Bourgogne, 9 Av. A. Savary, BP 47 870, 21078 Dijon Cedex, France; Corresponding author: christophe.finot@u-bourgogne.fr
[2] FEMTO-ST Institute, UMR 6174 CNRS-Université de Franche-Comté, 16 Route de Gray, 25030 Besancon, Cedex, France

*Received 26 June 2013*

**ABSTRACT:** *We analytically calculate and discuss the radio-frequency spectrum of the so called Akhmediev breathers (ABs), a class of nonlinear solutions of the nonlinear Schrödinger equation that governs the propagation in a single mode optical fiber. We propose a practical application of ABs to the field of ultra-wideband pulse generation.*
 Microwave Opt Technol Lett 56:664–667, 2014; View this article online at wileyonlinelibrary.com. DOI 10.1002/mop.28174

**Key words:** *nonlinear optics; ultra-wideband; fiber optics*

## 1. INTRODUCTION

Solitons on finite background (SFB) are solutions of the nonlinear Schrödinger equation (NLSE) that are pre.sently stimulating a renewed and widespread attention in nonlinear science. Even if their analytical expressions have been proposed for more than 25 years [1, 2], these nonlinear structures have been only recently identified, as promising prototypes of the infamous oceanic rogue waves [3, 4]. Indeed, due to the periodic exchange of energy between a continuous background and a localized structure, an initially small perturbation can exponentially grow into a brief and intense spike before disappearing. With the emergence of the field of optical rogue waves, theoretical and experimental works have confirmed that optical fibers represent an ideal testbed to easily generate and study SFB: Peregrine soliton [5], Akhmediev breathers (ABs) [6], or Kuznetsov-Ma solitons [7] have indeed been demonstrated, taking advantage of the widely available components for ultrafast optics. Connections with modulation instability [8], supercontinuum generation [9], and generation of ultrashort structures [10, 11] have recently been suggested, but at this stage, no solution has been designed to take advantage of the specific features of the SFB.

In this context, it sounds appealing to investigate the potential of ABs in the field of optical ultra-wideband pulse generation. Indeed, the temporal intensity or phase profiles [5, 12], the associated optical spectra [6], or the longitudinal recurrence [12, 13] have already been the subject of cautious theoretical and experimental works; the radio-frequency (RF) spectrum has not been exploited yet.

We analytically calculate in this contribution, the RF spectrum of ABs and demonstrate that they exhibit an ultra-wideband spectrum whose central frequency depends on the system parameters. This letter will be organized as follows: after having recalled the specific features of ABs, we provide the analytical expression of their RF spectrum. The evolution of the central frequency of this spectrum according to the parameters of the AB is then discussed. Finally, we compare the RF spectrum of ABs with spectra of usual Gaussian singlets and doublets for practical application to ultra-wideband pulse generation.

## 2. AKHMEDIEV BREATHERS

The propagation of light in optical fibers is described by the NLSE:

$$i\frac{\partial\psi}{\partial z}=i\frac{\beta_2}{2}\frac{\partial^2\psi}{\partial t^2}+i\gamma|\psi|^2\psi-\frac{\alpha}{2}\psi \tag{1}$$

where $z$ and $t$ denote the distance and retarded time (in the frame travelling at the group velocity) coordinates; $\beta_2$ and $\gamma$ are the group-velocity dispersion and the nonlinear Kerr coefficient, and $\psi(t,z)$ is the field envelope. In order to simplify the discussion, it is interesting to introduce the normalized distance, $\xi$, related to the dimensional distance via $\xi=z/L_{\mathrm{NL}}$ with the nonlinear length, $L_{\mathrm{NL}}=1/(\gamma P_0)$ for an initial plane wave of power, $P_0$.

AB is a class of solutions of the NLSE whose general expression (neglecting a term of propagating phase) reads as:

$$\psi(t,\xi)=\sqrt{P_0}\frac{(1-4a)\cosh(b\xi)+ib\sinh(b\xi)+\sqrt{2a}\cos(\omega_{\mathrm{mod}}t)}{\sqrt{2a}\cos(\omega_{\mathrm{mod}}t)-\cosh(b\xi)} \tag{2}$$

The parameters $a$ and $b$ are the normalized perturbation frequency and instability growth rate, and in dimensional units are given by $2a=1-(\omega_{\mathrm{mod}}/\omega_c)^2$ and $b=\sqrt{8a(1-2a)}$. Here $\omega_{\mathrm{mod}}$ denotes the dimensional modulation frequency in the range $0<\omega_{\mathrm{mod}}<\omega_c$, where $\omega_c^2=4\gamma P_0/|\beta_2|$. $a$ comprises values between 0 and 0.5, the value $a=0.5$ leads to the solution known as the Peregrine soliton.

At the point of maximum compression (i.e., at $\xi=0$), the compressed field is given by:

$$\psi(t,\xi=0)=\sqrt{P_0}\frac{(1-4a)+\sqrt{2a}\cos(\omega_{\mathrm{mod}}t)}{\sqrt{2a}\cos(\omega_{\mathrm{mod}}t)-1} \tag{3}$$

We compare the temporal intensity profiles obtained for a selection of three values of $a$ (0.25, 0.375, and 0.47). The value $a=0.25$ leads to the maximum of gain of the modulation instability process, whereas 0.47 represents the highest value of $a$ that has been to date experimentally reported [5]. The various examples are plotted on panels (1) of Figure 1 ($a=0.25$, 0.375, and 0.47 correspond to subplots a, b, and c, respectively). One can then clearly notice ultrashort and intense spikes of light lying over a continuous background as well as the increasing compression experienced for higher values of $a$.

The spectrum $s(\omega)$ of the AB [i.e., the Fourier transform of Eq. (2), $\omega$ being the angular frequency] is well documented [6] and exhibits a typical triangular shape when plotted on a logarithmic scale, highlighting the decrease of the frequency components. Due to the intrinsic temporal periodicity of ABs, the resulting spectrum is a comb with the amplitude, $s_n$, of the different frequency components given by [6] (here, factors of constant amplitude and phase are ignored):

$$\begin{cases} s_0(\xi)=\dfrac{ib\sinh(b\xi)+p^2\cosh(b\xi)}{\sqrt{\cosh^2(b\xi)-2a}}-1 \\ s_n(\xi)=\dfrac{ib\sinh(b\xi)+p^2\cosh(b\xi)}{\sqrt{\cosh^2(b\xi)-2a}}\left[\dfrac{\cosh(b\xi)-\sqrt{\cosh^2(b\xi)-2a}}{\sqrt{2a}}\right]^{|n|} \end{cases} \tag{4}$$

with $n\geq 1$ and the parameter, $p$, being $p=\sqrt{2}\omega_{\mathrm{mod}}/\omega_c$.

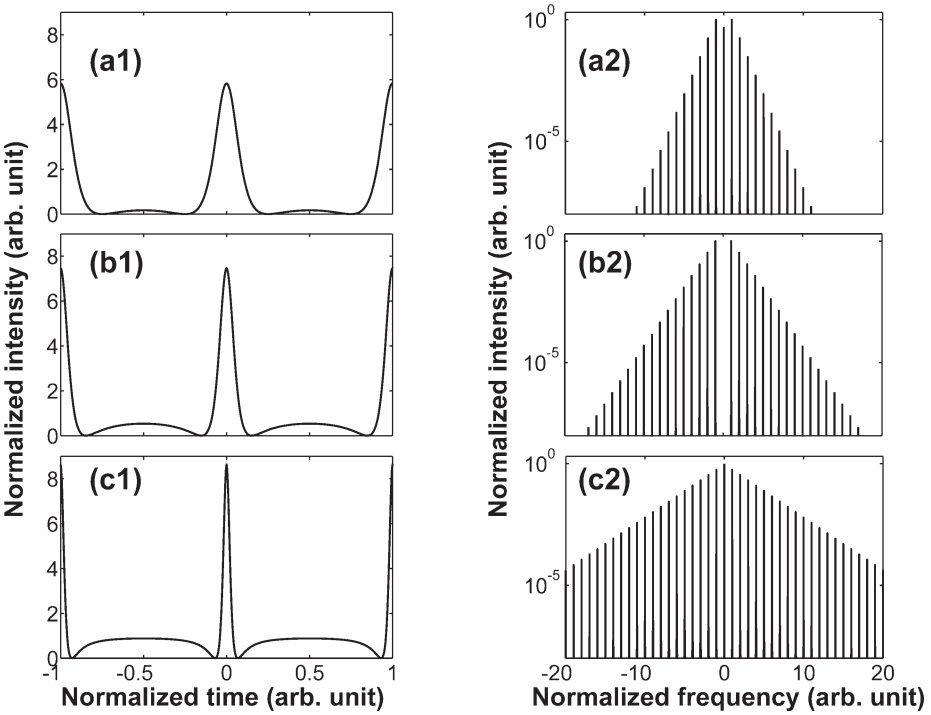


**Figure 1** Train of optical breathers for different values of $a$: $a = 0.25$, 0.375, and 0.47 are plotted in panels a, b, and c, respectively. The temporal intensity profiles at the point of maximum compression [Eq. (3)] are plotted in panels 1, whereas the optical spectra [square of Eq. (4)] are displayed in panels 2. Time is normalized with respect to the period of the pulse train, whereas frequency is normalized with respect to the repetition rate of the periodic signal

By stating

$$\begin{cases} r = \dfrac{i\,b\sinh(b\xi) + p^2\cosh(b\xi)}{\sqrt{\cosh^2(b\xi) - 2a}} \\ q = \dfrac{\cosh(b\xi) - \sqrt{\cosh^2(b\xi) - 2a}}{\sqrt{2a}} \end{cases}, \tag{5}$$

one can rewrite Eq. (4) into the following form :

$$\begin{cases} s_0 = r - 1 \\ s_n = r q^{|n|} \end{cases} \tag{6}$$

Results are illustrated on panels (2) of Figure 1 with the optical spectra [i.e., the square of the various coefficients (6)] obtained for different values of $a$. The continuously decreasing amplitude of the $s_n$ coefficients is confirmed, with a spectral extent increasing with higher values of $a$. We can note that the specific value of $a = 0.375$ leads to a cancelling of the central spectral component of the field.

### 3. RADIO-FREQUENCY SPECTRUM OF ABS

The RF spectrum $S(\omega)$ of ABs [i.e., the Fourier transform of the square of Eq. (2)] has been to date, fully unexplored and can be derived from Eqs. (6) taking into account that $S(\omega) = s(\omega) * \overline{s}(\omega)$ with $*$ being the convolution product and $\overline{s}$ being the complex conjugate of $s$. It leads to the general amplitude of the sideband $n \geq 1$ [$\mathrm{Re}(r)$ being the real part of $r$]:

$$S_n = q^{|n|}\left\{|r|^2\left(|n| + \frac{1+q^2}{1-q^2}\right) - 2\mathrm{Re}(r)\right\} \tag{7}$$

so that the overall envelope of the RF spectrum is given by:

$$S(\omega) = q^{\left|\frac{\omega}{\omega_{\mathrm{mod}}}\right|}\left\{|r|^2\left(\left|\frac{\omega}{\omega_{\mathrm{mod}}}\right| + \frac{1+q^2}{1-q^2}\right) - 2\mathrm{Re}(r)\right\} \tag{8}$$

The RF spectrums and the associated envelope corresponding to the fields investigated in the previous section are plotted on Figure 2. Compared to the simple algebraic decay of the optical spectrum tails, the RF spectrum undergoes a more complex evolution with frequency. The most important feature that can be made out is that the RF spectrum does not exhibit a monotonic decrease with increasing frequency: the RF envelope of the ABs has a local maximum in which the frequency depends on the value of $a$. For $a = 0.25$, the maximum of the RF spectrum is located at $\omega/\omega_{\mathrm{mod}} = 1$, whereas for $a = 0.375$ and 0.47, the maximum is shifted to the second and fourth spectral components, respectively.

One question that may arise is the influence of the propagation distance, $\xi$. In Figure 3(a), the longitudinal evolution of the RF spectrum envelope for $a = 0.47$ is plotted, outlines that the most significant shift is obtained at the point of maximum compression. From Eq. (8), one can evaluate more quantitatively, the frequency $\omega_{\mathrm{max}}$ at which the envelope is maximum:

$$\frac{\omega_{\mathrm{max}}}{\omega_{\mathrm{mod}}} = -\frac{1}{\ln q} - \frac{1+q^2}{1-q^2} + \frac{2}{r} \tag{9}$$

which can be simplified at the point of maximum of compression (where $r = 2\sqrt{1-2a}$ and $q = \frac{1-\sqrt{1-2a}}{\sqrt{2a}}$) into:

$$\begin{aligned} \frac{\omega_{\mathrm{max}}}{\omega_{\mathrm{mod}}}(\xi = 0) = {} & \frac{1}{\ln(2a)/2 - \ln\left(1-\sqrt{1-2a}\right)} \\ & - \frac{1-\sqrt{1-2a}}{2a-1+\sqrt{1-2a}} + \frac{1}{\sqrt{1-2a}} \end{aligned} \tag{10}$$

Results are plotted in Figure 3(b) and clearly points out that the central frequency continuously increases for increasing values of $a$.

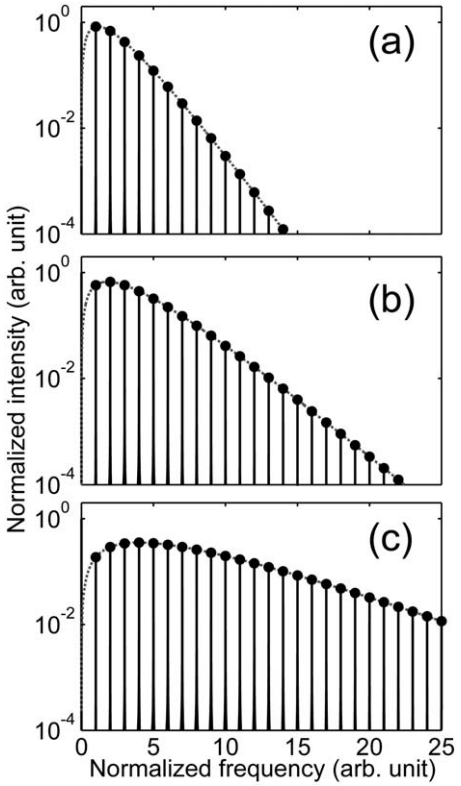


**Figure 2** RF spectra obtained for different values of $a = 0.25$, 0.375, and 0.47 (subplots a, b, and c, respectively). The numerical Fourier transform of Eq. (3) (black line) is compared with the analytical predictions of Eq. (7) (solid black circles) and with the envelope of the RF spectrum [grey solid line, Eq. (8)]

## 4. COMPARISON WITH SIMPLE SHAPES OF ULTRA-WIDEBAND PULSES

The generation of an ultrashort pulse train with a maximum of the RF spectrum shifted toward high frequency is a feature of interest in the context of ultra-wideband pulse generation [14]. Indeed, as the experimental setup involved in the generation of ABs is remarkably simple and can be easily scaled to repetitions rates of several tens of GHz [5], it is worthy to compare the performance of AB with the spectra of widely used pulse trains such as Gaussian singlet or doublets.

We have therefore considered here an AB, at the point of maximum compression, with a value of $a$ of 0.47. The resulting RF spectrum is compared on Figure 4(a) with Gaussian singlets and doublets having the same central frequency. The RF spectrum of an AB is slightly broader compared with the singlet, but significantly larger than the spectrum of a doublet. Corresponding intensity profiles are compared on Figure 4(b) and show that obtaining similar maximum frequencies of the RF spectrum requires a shorter structure in the case of ABs. For the same average power, the ABs exhibits a higher peak level, so that the pulsed part better distinguishes from the continuous background.

## 5. CONCLUSION

We have analytically calculated the RF spectrum of ABs and highlighted a significant feature of the soliton over finite background: contrary to their optical spectrum, their RF spectrum does not exhibit a monotonic evolving shape and the location of the maximum of this spectrum can be directly related to the $a$ parameter that takes both the fiber and light properties into

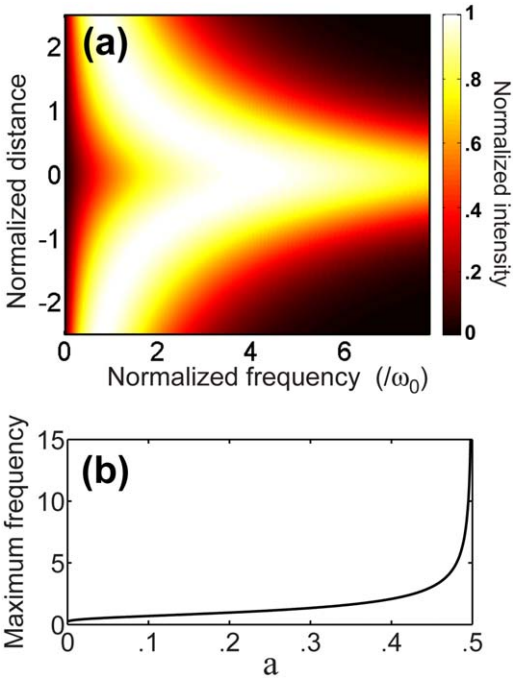


**Figure 3** (a) Longitudinal evolution of the envelope of the RF spectrum for $a = 0.47$. (b) Evolution of the frequency of the maximum of the RF spectrum with respect to the parameter $a$ at the point of maximum compression according to Eq. (10). [Color figure can be viewed in the online issue, which is available at wileyonlinelibrary.com]

account. To exploit this intrinsic property of the ABs, can be of interest for ultra-wideband pulse generation. Even if the performance of this pulse shape does not seem to compare favorably with usual Gaussian singlets and doublets, the ease of implementation of the experimental generation may constitute an attractive architecture if very high repetition rates are

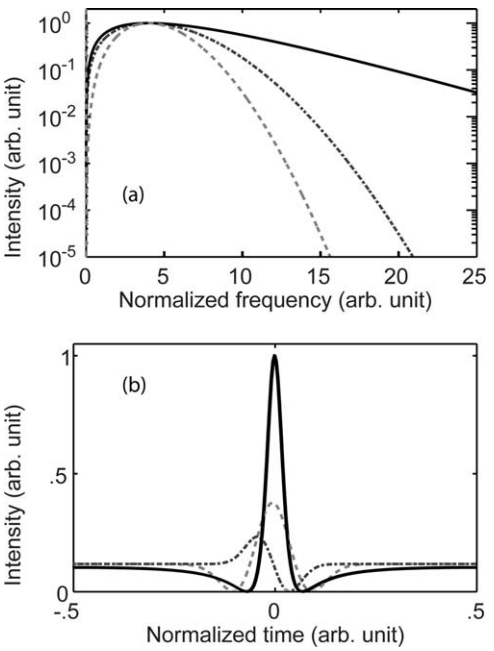


**Figure 4** (a) Comparison of the envelopes of the RF spectrum of a train of ABs (solid black line, $a = 0.47$) with the RF spectrum of a Gaussian singlet (dash-dotted line) and Gaussian doublet (dashed-grey line) having similar central frequencies. (b) Comparison of the corresponding temporal intensity profiles

targeted. The present discussion has been carried out in the context of passive fiber generation but breathers can also be observed in microresonators [15], paving the way to the all-optical and cost-effective generation on a compact optical chip. The proposed approach further stress all the benefits that can be obtained from the controlled shaping, occurring in a medium presenting dispersion and Kerr nonlinearity [16].


## ACKNOWLEDGMENTS

The authors thank Kamal Hammani, Bertrand Kibler, Julien Fatome, and G. Millot for stimulating discussions. The authors acknowledge the financial support of the Conseil Regional de Bourgogne (Pari Photcom) and the Agence Nationale de la Recherche (project SO FAST, ANR-11-EMMA-0005 and OPTIROC, ANR-12-BS04-0011). The authors also thank the funding of the Labex ACTION program (ANR-11-LABX-01-01).l


## REFERENCES


1. E.A. Kuznetsov, Solitons in a parametrically unstable plasma, Dokl Akad Nauk SSSR 22 (1977), 507–508.
2. N.N. Akhmediev and V.I. Korneev, Modulation instability and periodic-solutions of the nonlinear Schrödinger equation, Theor Math Phys 69 (1986), 1089–1093.
3. N. Akhmediev, A. Ankiewicz, and M. Taki, Waves that appear from nowhere and disappear without a trace, Phys Lett A 373 (2009), 675–678.
4. M. Onorato, D. Proment, G. Clauss, and M. Klein, Rogue waves: From nonlinear Schrödinger breather solutions to sea-keeping test, PLoS ONE 8 (2013), e54629.
5. K. Hammani, B. Kibler, C. Finot, P. Morin, J. Fatome, J.M. Dudley, and G. Millot, Peregrine soliton generation and breakup in standard telecommunications fiber, Opt Lett 36 (2011), 112–114.
6. K. Hammani, B. Wetzel, B. Kibler, J. Fatome, C. Finot, G. Millot, N. Akhmediev, and J.M. Dudley, Spectral dynamics of modulation instability described using Akhmediev breather theory, Opt Lett 36 (2011), 2140–2142.
7. B. Kibler, J. Fatome, C. Finot, G. Millot, G. Genty, B. Wetzel, N. Akhmediev, F. Dias, and J.M. Dudley, Observation of Kuznetsov-Ma soliton dynamics in optical fibre, Sci Rep 2 (2012), 463.
8. M. Erkintalo, K. Hammani, B. Kibler, C. Finot, N. Akhmediev, J.M. Dudley, and G. Genty, Higher-order modulation instability in nonlinear fiber optics, Phys Rev Lett 107 (2011), 253901.
9. J.M. Dudley, G. Genty, F. Dias, B. Kibler, and N. Akhmediev, Modulation instability, Akhmediev breathers and continuous wave supercontinuum generation, Opt Express 17 (2009), 21497–21508.
10. C. Mahnke and F. Mitschke, Possibility of an Akhmediev breather decaying into solitons, Phys Rev A 85 (2012), 033808.
11. J. Fatome, B. Kibler, and C. Finot, High-quality optical pulse train generator based on solitons on finite background, Opt Lett 38 (2013), 1663–1665.
12. N. Devine, A. Ankiewicz, G. Genty, J. Dudley, and N. Akhmediev, Recurrence phase shift in Fermi–Pasta–Ulam nonlinear dynamics, Phys Lett A 375 (2011), 4158–4161.
13. G. Van Simaeys, P. Emplit, and M. Haelterman, Experimental demonstration of the Fermi–Pasta–Ulam recurrence in a modulationally unstable optical wave, Phys Rev Lett 87 (2001), 033902.
14. Y. Jianping, Z. Fei, and W. Qing, Photonic generation of ultrawideband signals, J Lightwave Technol 25 (2007), 3219–3235.
15. A.B. Matsko, A.A. Savchenkov, and L. Maleki, On excitation of breather solitons in an optical microresonator, Opt Lett 37 (2012), 4856–4858.
16. K. Hammani, B. Kibler, J. Fatome, S. Boscolo, G. Genty, J.M. Dudley, G. Millot, and C. Finot, Nonlinear spectral shaping and optical rogue events in fiber-based systems, Opt Fiber Technol 18 (2012), 248–256.




# A CROSS-STITCH GEOMETRY-BASED MULTIBAND FRACTAL ANTENNA


**Balwinder S. Dhaliwal,[1] Shyam S. Pattnaik,[2] and Jasmine Boparai[3]**

[1] Guru Nanak Dev Engineering College (GNDEC), Ludhiana, Punjab, India; Corresponding author: bs_dhaliwal@gndec.ac.in
[2] National Institutes of Technical Teachers' Training and Research (NITTTR), Chandigarh, India
[3] Chitkara University, Barotiwala, Himachal Pradesh, India



*Received 3 July 2013*



**ABSTRACT:** *Fractal antennas have the characteristics of radiating in the multiple frequency bands due to self-similarity property. Using the same, a new fractal patch antenna is presented in this article. The antenna is based on cross-stitch geometry. The simulation and measured results show that the proposed antenna has multiband performance with sufficient gain and high directivity.* © 2014 Wiley Periodicals, Inc. Microwave Opt Technol Lett 56:667–671, 2014; View this article online at wileyonlinelibrary.com. DOI 10.1002/mop.28177



**Key words:** *fractal antenna; multiband; cross-stitch geometry*


## 1. INTRODUCTION

Fractal antennas are relatively a new area in the antennas domain. The fractal patch antennas due to their shapes have proved to be a solution provider for multiband and miniaturized antenna. They have space filling property which results in miniaturized antennas, and the self similarity characteristic of fractal antennas results in multiband performance [1]. The advantages of fractal antennas include input impedance matching, efficiency and effectiveness, and improved directivity [1].

Different geometries have been proposed by researchers in recent years. The Sierpinski's gasket proposed by Puente et al. [2] is one of the early fractal multiband monopole antennas. This antenna shows similar behavior of input return loss and radiation pattern for several frequency bands. This geometry is most studied geometry in fractal antenna research. A triangular fractal antenna in which each side of the triangle is having triangular notches at the log-periodic interval is presented in [3]. The Van Koch fractal monopole antenna with improved bandwidth and radiation resistance is another example of fractal antenna proposed by Puente et al. [4]. The authors of [5] proposed a fractal antenna based on Hilbert curves which is less than $\lambda/10$ in size as compared to a dipole of resonant length of $\lambda/2$ with similar performance. A self similar circularly polarized fractal antenna based on square shape is explored by [6]. This antenna has multiband performance and the first mode frequency is lower than that of a square microstrip patch antenna of same size. A multiband fractal antenna based on Sierpinski carpet geometry is described by [7]. A fractal antenna geometry based on "+" sign investigated in [8] has been shown to possess size reduction and multiband performance. Aziz et al. [9] proposed a microstrip line-fed multiband fractal-like antenna implemented using a partial ground plane. A novel circular-hexagonal fractal antenna for super wide band applications ranging from 2.18 to 44.5 GHz is investigated in [10].

The above discussion makes it clear that different fractal structures are explored in the past and search for new geometrics is still on. A new fractal antenna based on cross-stitch is presented in this article. The antenna shows multiband characteristics with high directive gain. Section 2 describes the geometry and dimensions of proposed antenna. The results